Domenico A.G. Dell’Aglio

Tutor: Prof. Antonio Iodice

XXXII Cycle - III year presentation

Synthetic Aperture Radar for Natural Hazards Observation

from Acquisition Geometry to Applications to Landslides

Università degli Studi di Napoli Federico II

My personal background

- BSc in **Telecommunications Engineering** - University of Naples “Federico II”, May 2012
- MSc in **Telecommunications Engineering** - University of Naples “Federico II”, January 2016

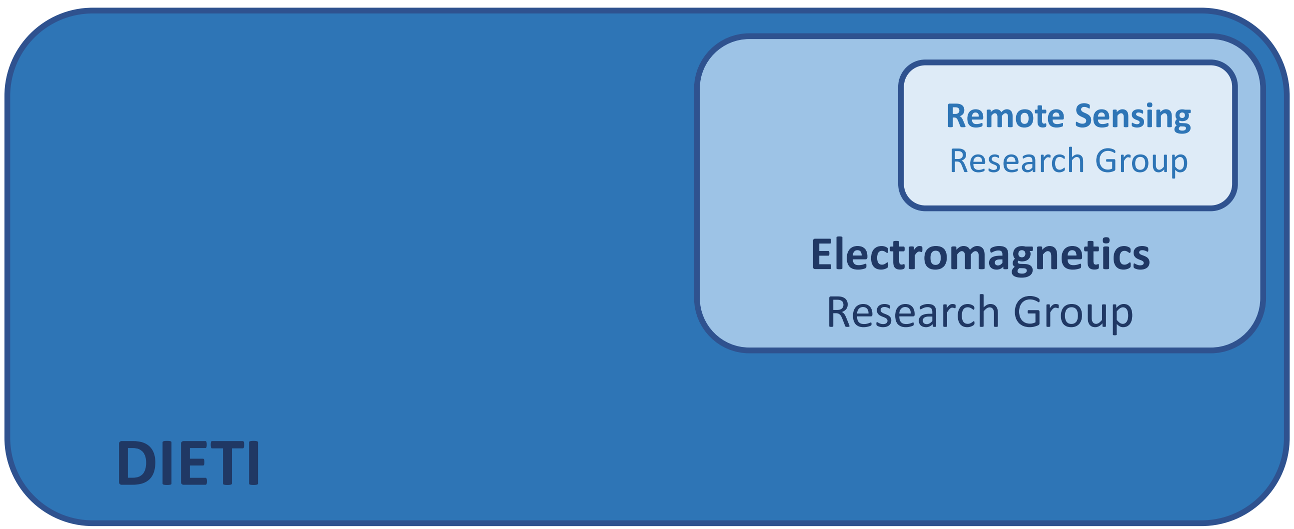

My personal background

- Training Activities:

Student: Domenico A G. Dell'Aglio								**Tutor: Prof. Antonio Iodice**							**Cycle XXXII**											
domenicoantoniogiuseppe.dellaglio@unina.it								antonio.iodice@unina.it																		
	Credits year 1								**Credits year 2**								**Credits year 3**									
		1	2	3	4	5	6			1	2	3	4	5	6			1	2	3	4	5	6			
	Estimated	bimonth	bimonth	bimonth	bimonth	bimonth	bimonth	**Summary**	**Estimated**	bimonth	bimonth	bimonth	bimonth	bimonth	bimonth	**Summary**	**Estimated**	bimonth	bimonth	bimonth	bimonth	bimonth	bimonth	**Summary**	**Total**	**Check**
Modules	**20**					3	15	**18**	**10**	3		9		0,4	3	**15,4**	**0**	1,2						**1,2**	**34,6**	**30-70**
Seminars	**5**				1,3	1,6	2,3	**5,2**	**5**	2,3	0,9	0,2	1,2	1,1	0,2	**5,9**	**0**	0,4	1,3	0,6				**2,3**	**13,4**	**10-30**
Research	**35**	10	10	10	8,7	5,4		**44,1**	**45**	4,7	9,1	0,8	8,8	8,5	6,8	**38,7**	**60**	8,4	8,7	9,4	10	10	10	**56,5**	**139,3**	**80-140**
	60	10	10	10	10	10	17,3	**67,3**	**60**	10	10	10	10	10	10	**60**	**60**	10	10	10	10	10	10	**60**	**187,3**	**180**

- Collaborations:
  - ✓ Benecon S.C.aR.L. - Istitutional Partner of the Forum UNESCO University and Heritage
  - ✓ Progressive Systems S.r.l. - ESA Research and Service Support

Outline

PART I

- Introduction
  - Remote Sensing and Synthetic Aperture Radar (SAR)
- SAR Acquisition Modes
  - Unified SAR Raw Signal Formulation
  - Application to Simulation: TOPSAR
  - Results and Computational Complexity

PART II

- Terrain Displacement Measurements via SAR
  - Introduction and Motivations
- DInSAR Multi-Temporal Analysis
  - Methodology and Implementation
  - Results
- Sub-Pixel Offset Tracking (SPOT) Technique
  - Methodology and Implementation
  - Results

CONCLUSIONS

Outline

PART I

- Introduction
  - Remote Sensing and Synthetic Aperture Radar (SAR)
- SAR Acquisition Modes
  - Unified SAR Raw Signal Formulation
  - Application to Simulation: TOPSAR
  - Results and Computational Complexity

PART II

- Terrain Displacement Measurements via SAR
  - Introduction and Motivations
- DInSAR Multi-Temporal Analysis
  - Methodology and Implementation
  - Results
- Sub-Pixel Offset Tracking (SPOT) Technique
  - Methodology and Implementation
  - Results

CONCLUSIONS

Remote Sensing - Motivations

Provides unique information to solve social challenges of global dimension

Climate Change

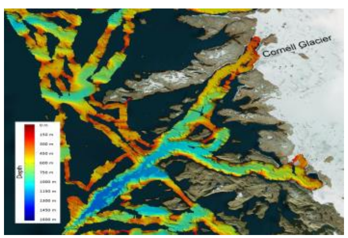

Glacier Motion

Megacities

Urban Planning

Hazards

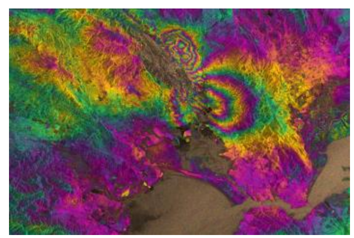

Vulcano Monitoring

Mobility

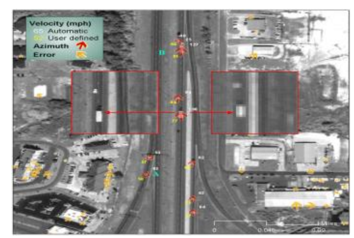

Traffic Monitoring

Sustainability

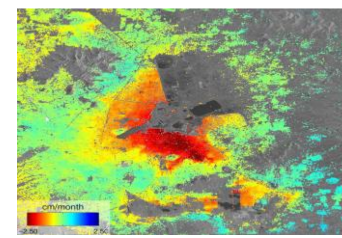

Subsidence

Remote Sensing Sensors

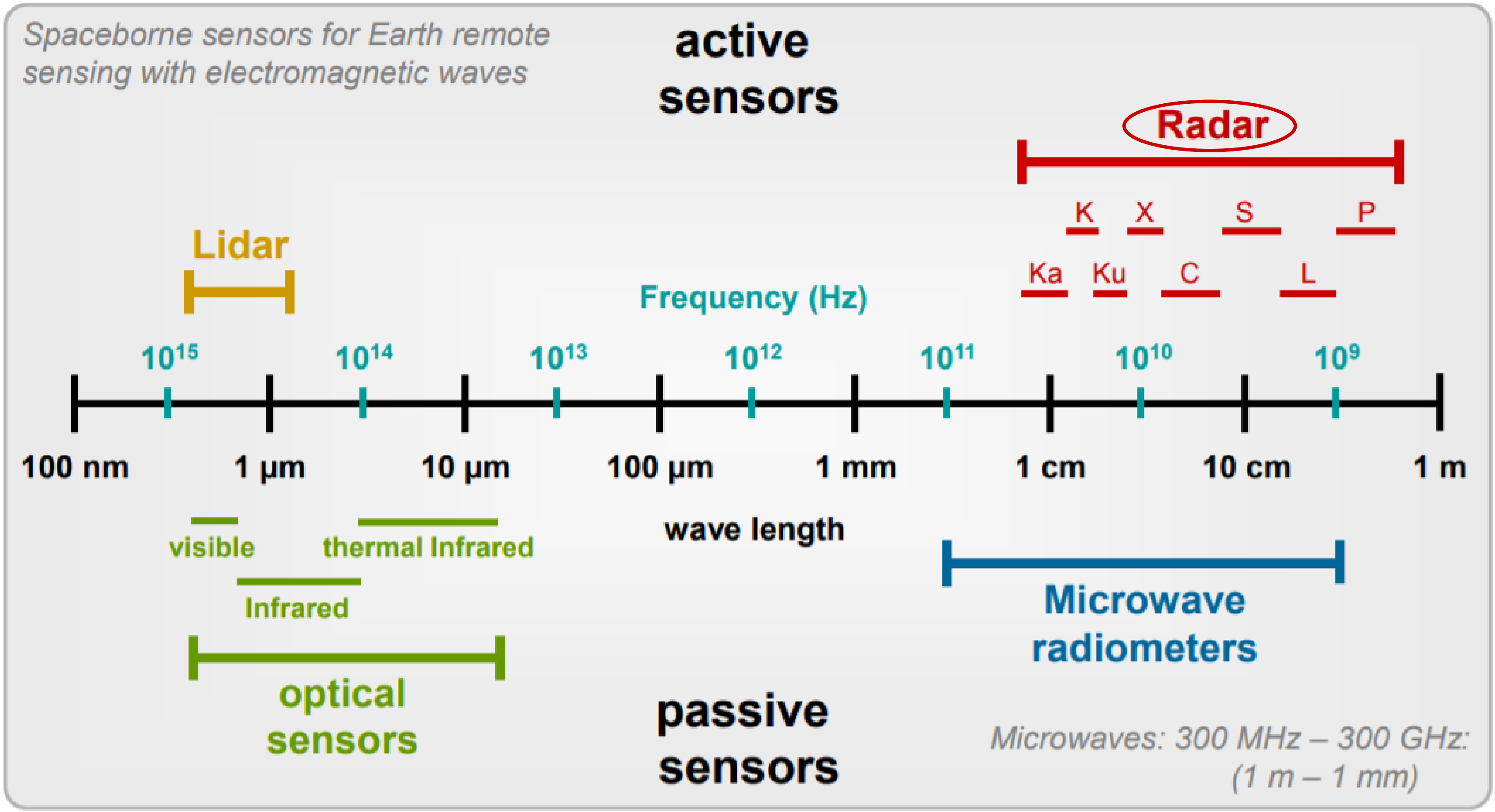

RAR Basic Principles

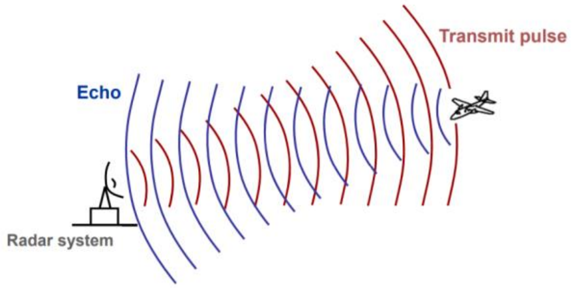

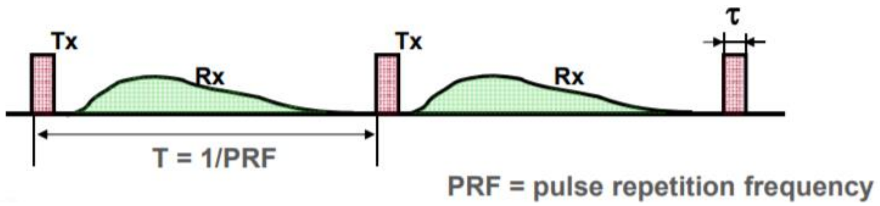

Side-looking geometry

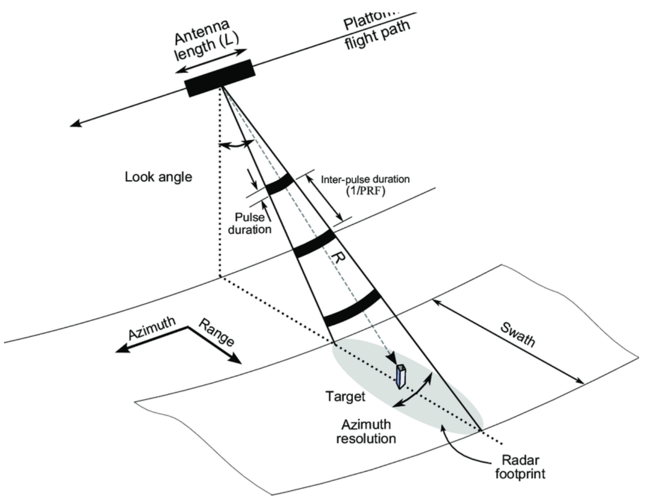

Aperture means the opening used to collect the reflected energy from the observed object. In the case of the radar imaging this is the antenna length

For RAR systems **only the amplitude** of each returned echo is measured and processed

RAR Basic Principles

- **Slant range resolution** depends on the transmitted pulse duration τ (i.e., the bandwidth)

$$\Delta r = \frac{c\tau}{2}$$

- **Azimuth resolution** depends, in general, on three parameters. But for a sensor working at a certain frequency and at a fixed high (i.e., fixed R), it depends just on the azimuth antenna length L

$$\Delta x = R\frac{\lambda}{L}$$

- *Example:* for a spaceborne sensor working at X-Band, 25 MHz bandwidth, with $L = 12\ m$ and $R = 800\ km$

$\Delta r = 6\ m$

$\Delta x = 2\ km$!

improvement →

Modulation: e.g., **chirp**

SAR systems

SAR Basic Principles

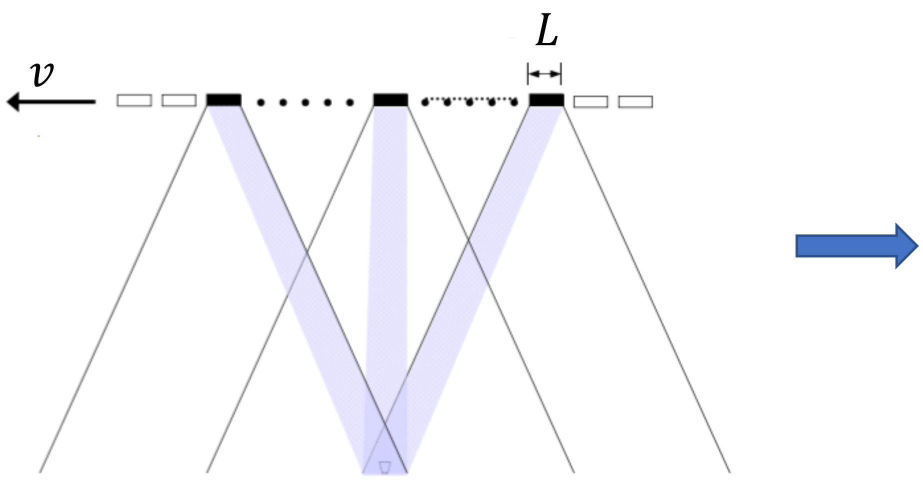

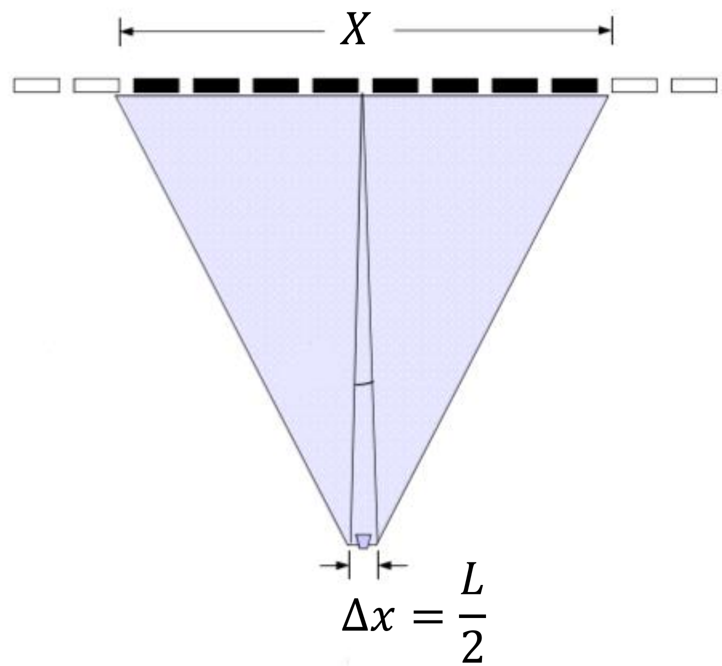

- Pulsed radar system
- Coherent system: **phase information** is preserved
- 2D imaging
- **Azimuth resolution** becomes independent on range distance

Outline

PART I

- Introduction
  - Remote Sensing and Synthetic Aperture Radar (SAR)
- SAR Acquisition Modes
  - Unified SAR Raw Signal Formulation
  - Application to Simulation: TOPSAR
  - Results and Computational Complexity

PART II

- Terrain Displacement Measurements via SAR
  - Introduction and Motivations
- DInSAR Multi-Temporal Analysis
  - Methodology and Implementation
  - Results
- Sub-Pixel Offset Tracking (SPOT) Technique
  - Methodology and Implementation
  - Results

CONCLUSIONS

SAR Acquisition Modes

Spotlight

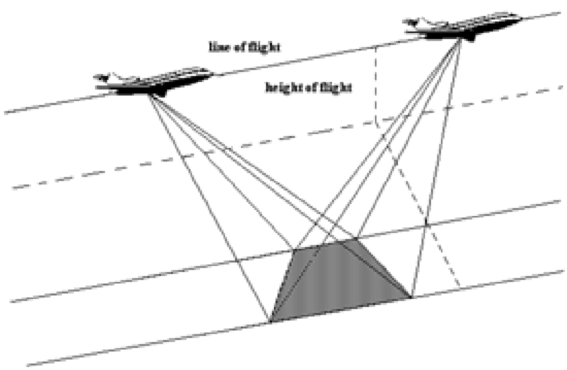

Sliding-Spotlight

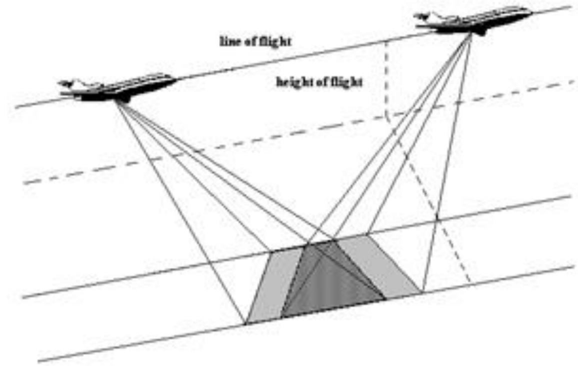

Stripmap

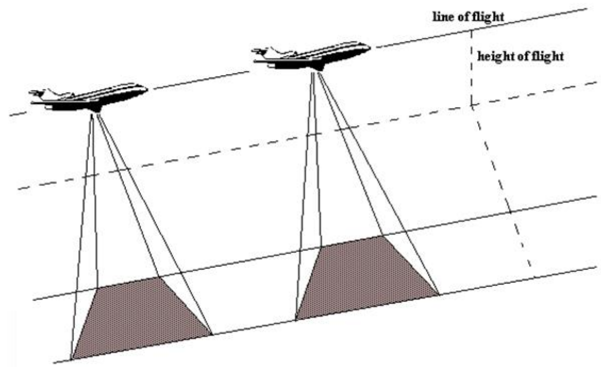

ScanSAR

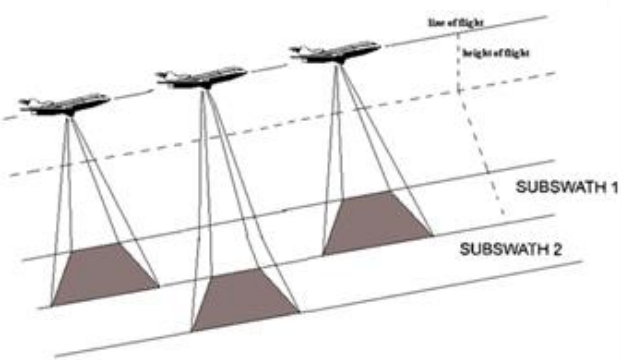

TOPSAR

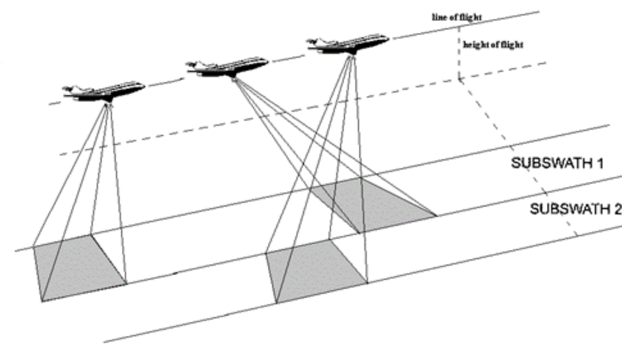

Unified SAR Raw Signal Formulation

TOPSAR

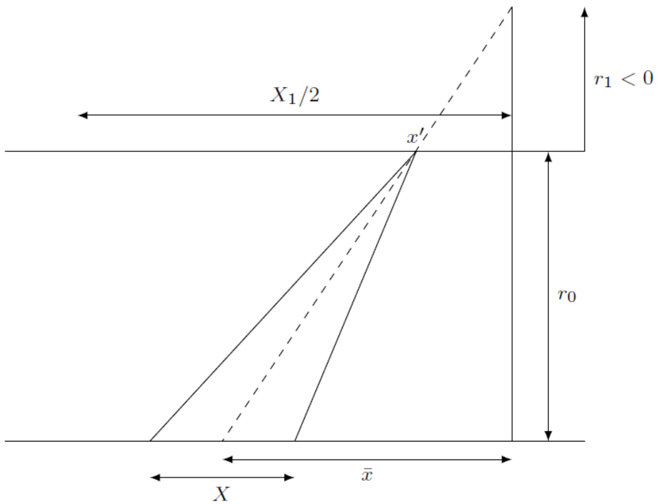

Sliding-Spotlight

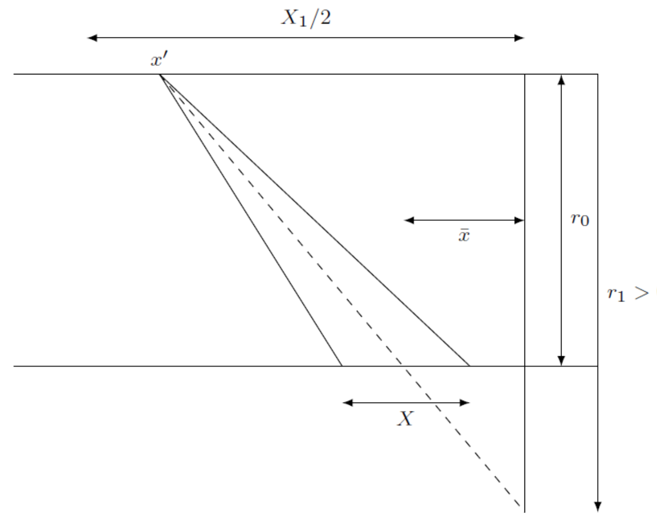

$$A = \frac{r_1 - r_0}{r_1}$$

$$\omega_a = \frac{v}{r_0}(1 - A) \qquad v_f = Av \qquad \bar{x} = Ax' \qquad w\left(\frac{Ax' - x}{X}\right)$$

Unified SAR Raw Signal Formulation

Introducing the following factor

$$B = \frac{X}{X_1}$$

we can rewrite:

Range of values	Acquisition modes
$A = 0$	spotlight
$0 < A < 1$	sliding spotlight
$A = 1, B \ll 1$	stripmap
$A = 1, B > 1$	scanSAR
$A > 1$	TOPSAR
$-1 \leq A \leq 0$	inverse sliding spotlight
$A < -1$	inverse TOPSAR

- SAR system **Impulse Response**:

$$g(x', r' - r; x, r) = e^{-j\frac{4\pi}{\lambda}\Delta R} e^{-j\frac{4\pi}{\lambda}\frac{\Delta f/f}{c\tau}(r'-r-\Delta R)^2} rect\left[\frac{r' - r - \Delta R}{c\tau/2}\right] w^2\left(\frac{Ax' - x}{X}\right) rect\left[\frac{x'}{X_1}\right]$$

- SAR system **Transfer Function**:

$$G(\xi, \eta; x, r) = e^{j\frac{\eta^2}{4b}} e^{j\frac{\xi^2 (r/r_0)}{4a(1 + \eta\lambda/4\pi)}} rect\left[\frac{\eta}{bc\tau}\right] w^2\left(\frac{A\xi - 2a(A-1)x}{2aX}\right) rect\left[\frac{B(\xi - 2ax)}{2aX}\right]$$

Application to Simulation - TOPSAR

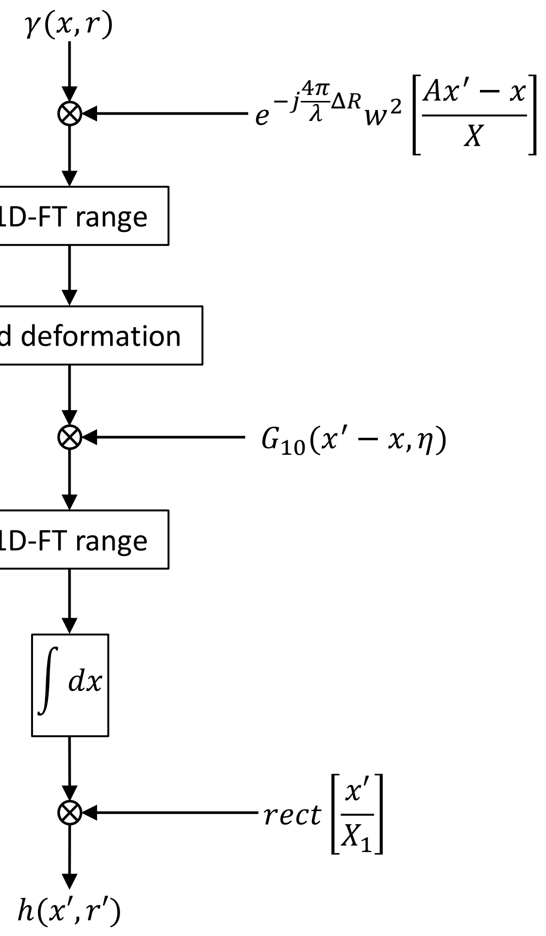

	Spaceborne	**Airborne**
Platform height	$693\ km$	$6\ km$
Platform velocity	$7{,}5\ km/s$	$0{,}142\ km/s$
Look angle	$24°$	$50°$
Azimuth antenna length	$12\ m$	$0{,}9\ m$
Range antenna length	$0{,}7\ m$	$0{,}141\ m$
Carrier frequency	$5{,}405\ GHz$	$5{,}31\ GHz$
Pulse duration	$50\ \mu s$	$7\ \mu s$
Pulse bandwidth	$50\ MHz$	$37{,}5\ MHz$
Sampling frequency	$50\ MHz$	$37{,}5\ MHz$
Pulse repetition frequency	$1642\ Hz$	$329\ Hz$
A	$2{,}9$	$2{,}9$
B	$0{,}5$	$0{,}5$
Azimuth resolution	$17{,}4\ m$	$1{,}302\ m$
Ground range resolution	$7{,}4\ m$	$5{,}221\ m$
Raw signal azimuth size	$1537\ pixels$	$2716\ pixels$
Raw signal range size	$15040\ pixels$	$1488\ pixels$

Simulation Results - Single Point

Time vs **Proposal** at scene center: $(x = 0, r = r_0)$

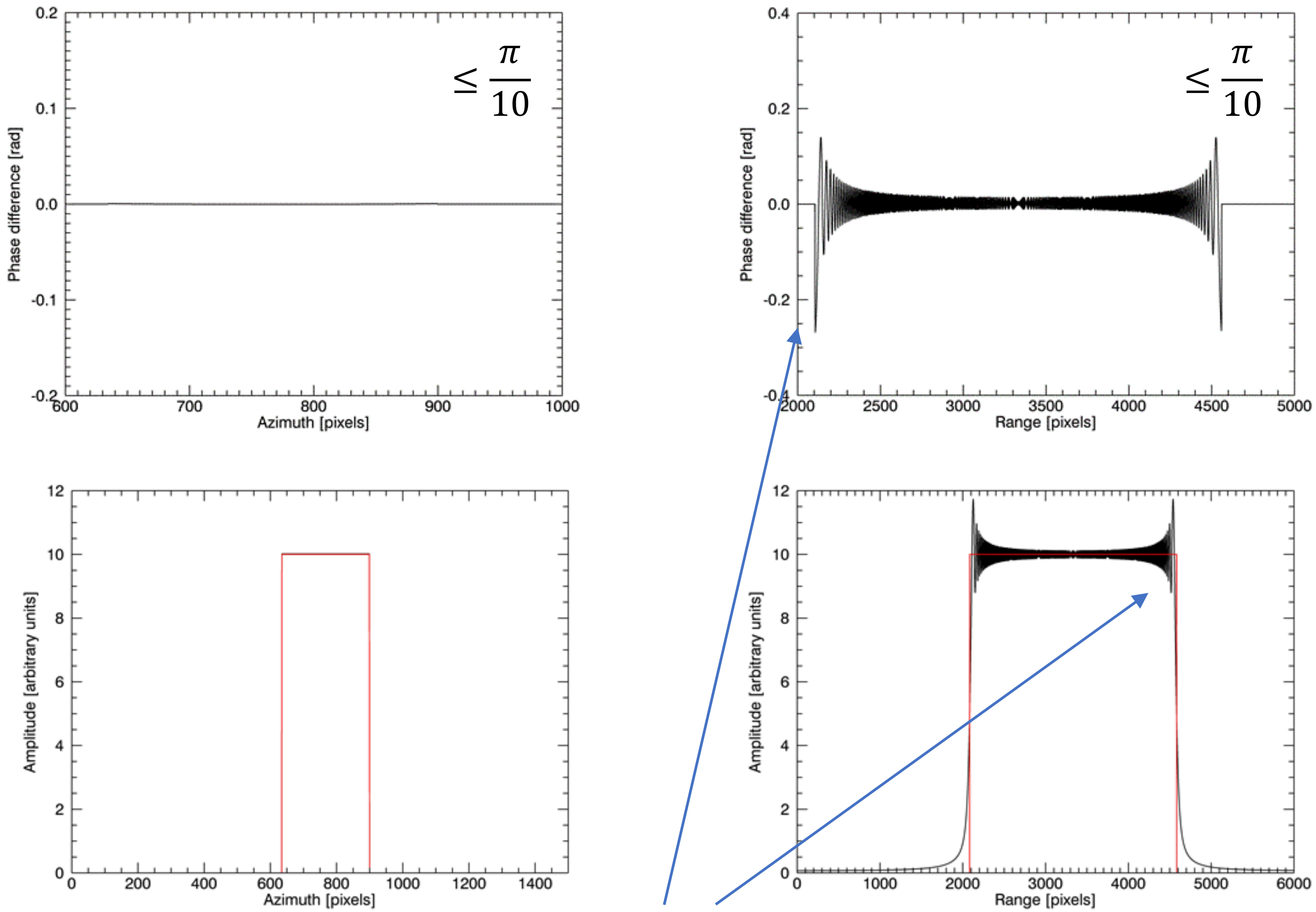

Stationary phase method

Simulation Results - Single Point

Time vs **Proposal** at near range scene border: $(x = -8000\ m, r = r_0 - 18300\ m)$

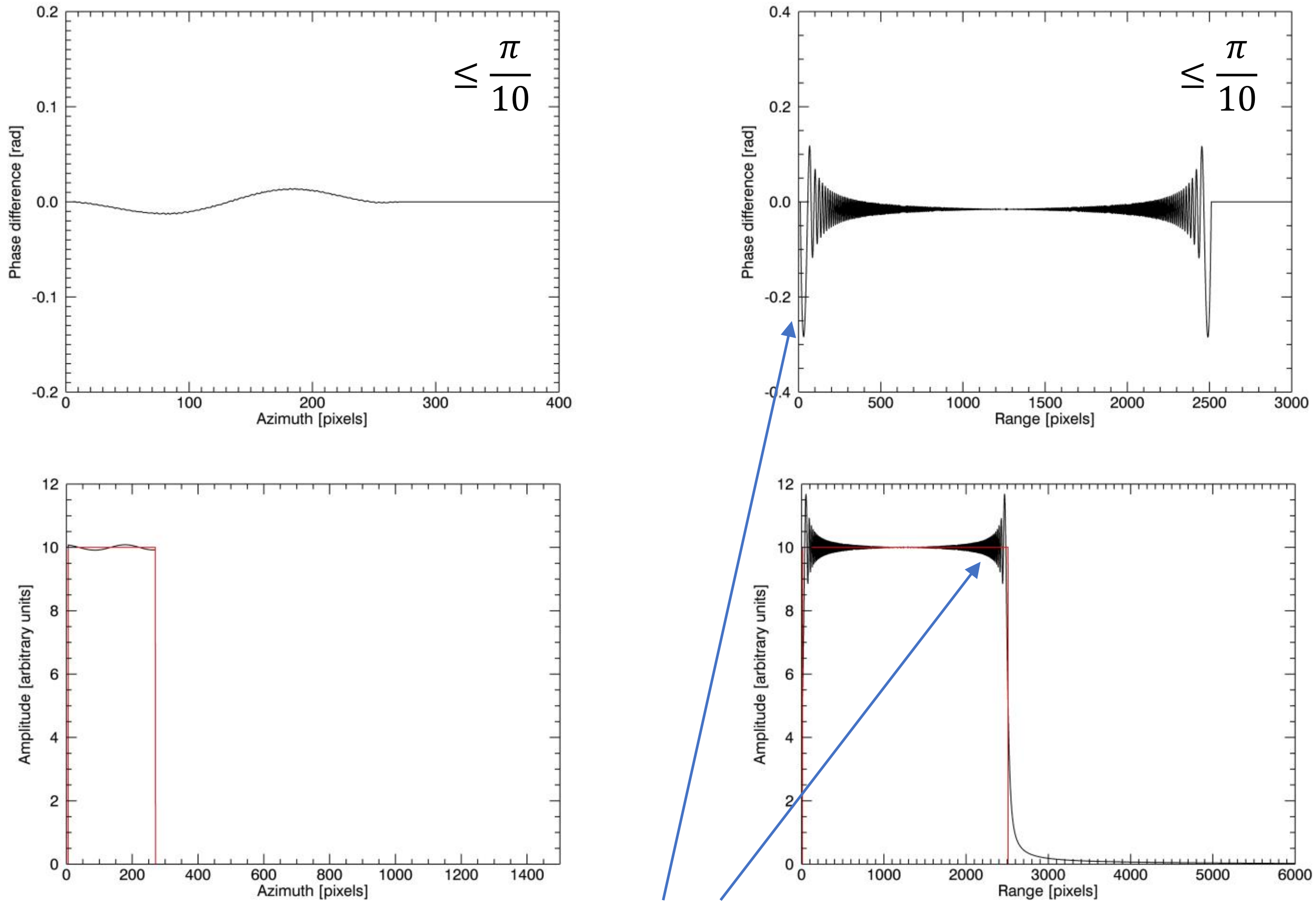

Stationary phase method

Simulation Results - Wide Scenes

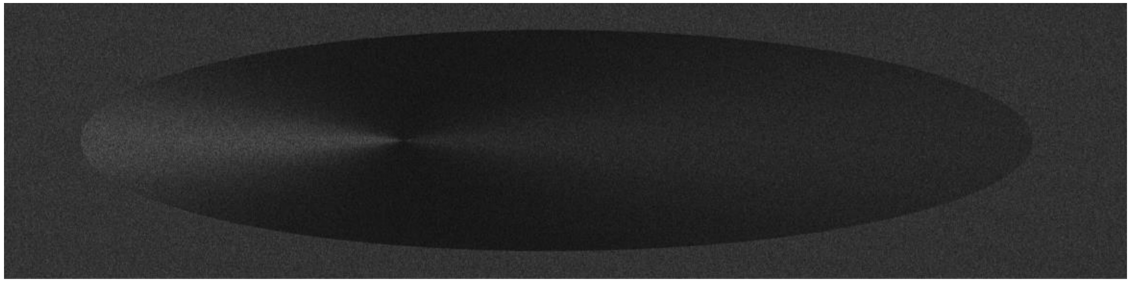

Amplitude image obtained by focusing a simulated raw signal of a canonical extended scene constituted by a cone over a flat plane.

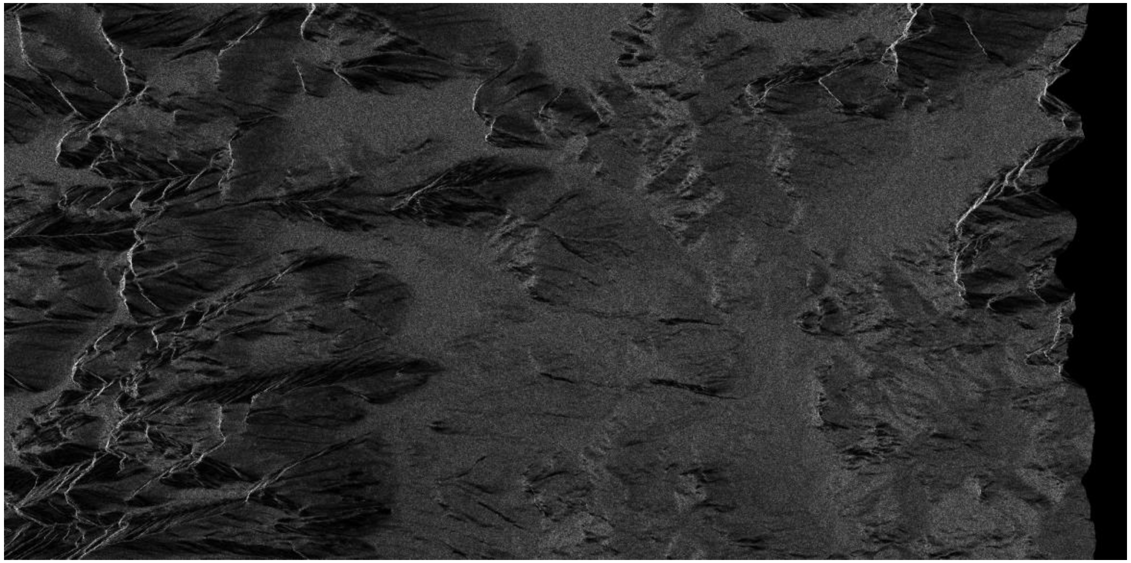

Amplitude image obtained by focusing a simulated raw signal of a real extended scene: the Apennines area in Campania, Italy. A multilook of 2 has been applied in the range direction to obtain an almost square pixel.

Simulation Results - Path Deviation

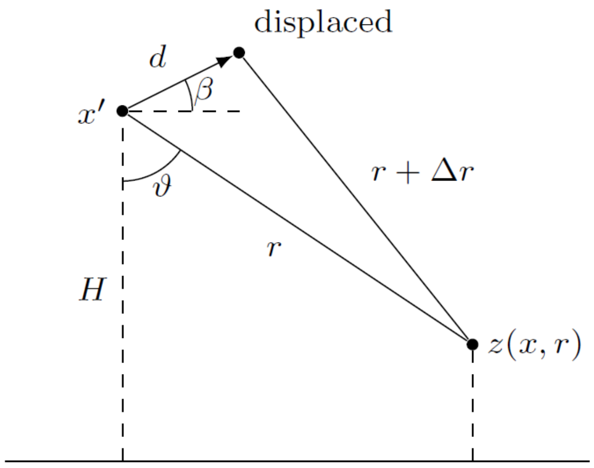

Scene center: $(x = 0, r = r_0)$

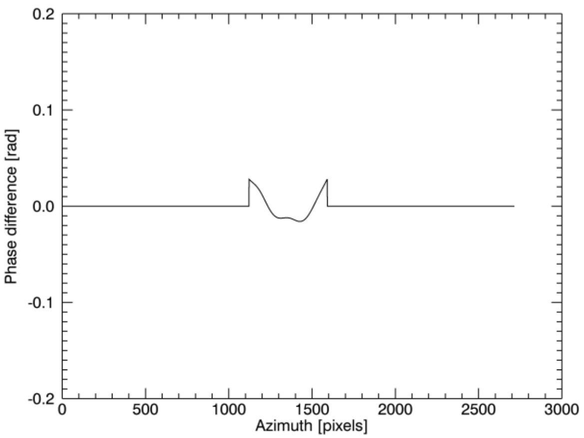

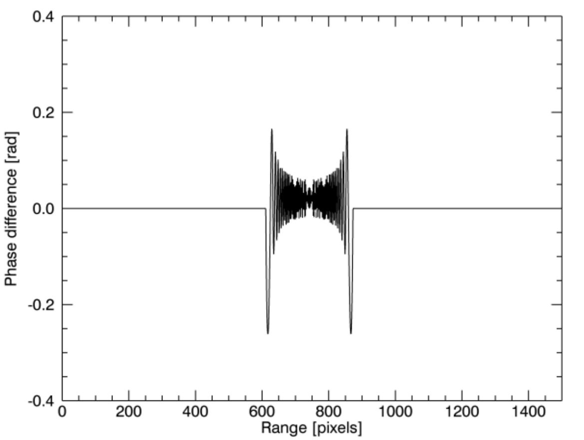

Sinusoidal deviations from the ideal flight direction, with $1\ m$ amplitude (projected along the LOS) and a period of $157\ m$

Computational Complexity

- The computational complexity is measured comparing the number of complex multiplications of the full Time-Domain approach (N_{TD}) with that one of the proposed approach (N_{1DFD})

- N_1 = number of pulses within a burst length X_1
- N = number of scene pixels within one azimuth footprint X
- N_r = number of range pixels within the range swath S_r
- N_τ = number of samples of the transmitted pulse duration τ

$$N_{TD} \approx N_1 N N_r N_\tau$$

$$N_{1DFD} \approx N_1 N N_r (2 + \log_2 N_r)$$

$$\Rightarrow \quad \frac{N_{1DFD}}{N_{TD}} = \frac{2 + \log_2 N_r}{N_\tau}$$

- <u>*Example*</u>: $N_r = 8192$ and $N_\tau = 4096 \Rightarrow \frac{N_{1DFD}}{N_{TD}} = \frac{1}{273}$

Outline

PART I

- Introduction
  - Remote Sensing and Synthetic Aperture Radar (SAR)
- SAR Acquisition Modes
  - Unified SAR Raw Signal Formulation
  - Application to Simulation: TOPSAR
  - Results and Computational Complexity

PART II

- Terrain Displacement Measurements via SAR
  - Introduction and Motivations
- DInSAR Multi-Temporal Analysis
  - Methodology and Implementation
  - Results
- Sub-Pixel Offset Tracking (SPOT) Technique
  - Methodology and Implementation
  - Results

CONCLUSIONS

Introduction and Motivations

Increasing number of **satellites** → The remote sensing products → **Earth Monitoring**

- The **Italian Space Agency** (ASI) has launched the **COSMO-SkyMed** satellites;
- Four SAR satellites sensors working at **X-band**;
- Three basic acquisition modes: **Spotlight**, **Stripmap**, **ScanSAR**.

- The **European Space Agency** (ESA) has recently launched the twin satellites **Sentinel-1**;
- Two SAR satellites (S1-A/B) working at **C-Band**;
- Four basic acquisition modes: **Stripmap**, **Interferometric Wide-Swath** (IW), **Extra Wide-Swath** (EW), **Wave** (WV)

Both the data are useful in **landslide monitoring**, exploiting **Time Series Analysis**

Introduction and Motivations

Infrastructures monitoring/slow landslides at large scale:

- Demanding on field campaigns using dedicated instruments and/or GPS
- **Differential SAR Interferometry (DInSAR)**: it exploits phase information

Sentinel 1 - DInSAR

Pros	*Cons*
High (subwavelength) displacement accuracy	**Decorrelation in vegeted areas**
Wide coverage	1D measurement
Temporal evolution of deformations	Sensitivity to atmospheric effects
	Maximum measurable displacement gradient

Introduction and Motivations

Vegeted areas/fast landslides monitoring:

- **Sub-Pixel Offset Tracking (SPOT)**: it exploits only amplitude information
- Successfully applied on glaciers → on landslides?

COSMO-SkyMed - SPOT

Pros	*Cons*
Fast slides	**Lower (sub-pixel) accuracy**
2D measurement	Slow slides
Less sensitive to decorrelation in vegeted areas	
No atmospheric effects	

Outline

PART I

- Introduction
  - Remote Sensing and Synthetic Aperture Radar (SAR)
- SAR Acquisition Modes
  - Unified SAR Raw Signal Formulation
  - Application to Simulation: TOPSAR
  - Results and Computational Complexity

PART II

- Terrain Displacement Measurements via SAR
  - Introduction and Motivations
- DInSAR Multi-Temporal Analysis
  - Methodology and Implementation
  - Results
- Sub-Pixel Offset Tracking (SPOT) Technique
  - Methodology and Implementation
  - Results

CONCLUSIONS

DInSAR Multi-Temporal Analysis

Study Areas and Dataset

Fiumicino - Ascending Orbit

Fiumicino - Descending Orbit

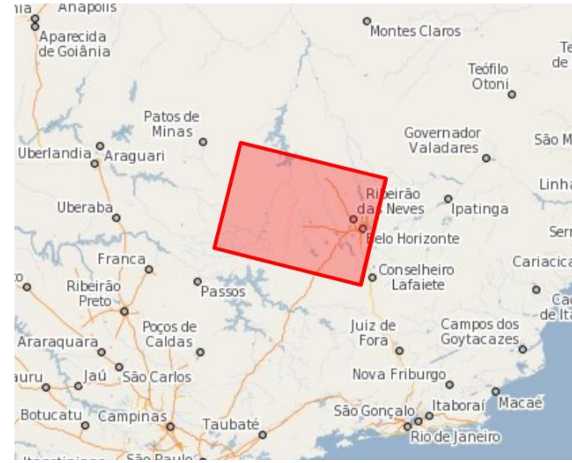

Brumadinho - Descending Orbit

Sentinel-1 dataset	Fiumicino airport		Brumadinho dam	
	Ascending	Descending	Ascending	Descending
# of acquisitions	185	114	-	108
Track	117	95	-	53
Acquisition period	10/2014 – 02/2019		01/05/2015 – 22/01/2019	

DInSAR Multi-Temporal Analysis

Methodology[1]

- N = # of SAR images
- M = # of interferograms

$$\Longrightarrow \begin{cases} \boldsymbol{\varphi} = & \text{vector of } N \textbf{ unknown} \text{ phase values} \\ \boldsymbol{\delta\varphi} & : \delta\varphi_i \triangleq \varphi(t_{IM_i}) - \varphi(t_{IS_i}) \quad \forall i = 1, \dots, M \end{cases}$$

where $\boldsymbol{IM}$ and $\boldsymbol{IS}$ are the index vectors corresponding to the acquisition time-indices associated to the Master and Slave pairs.
So, for each pixel of the M generated interferograms, we have to solve the following matrix-form equation

$$\boldsymbol{A\varphi} = \boldsymbol{\delta\varphi} \Leftrightarrow \boldsymbol{Bv} = \boldsymbol{\delta\varphi}$$

if $\boldsymbol{A}$ is a diagonal block matrix and

$$\boldsymbol{v} \triangleq \left[\frac{\varphi_1}{t_1 - t_0}, \dots, \frac{\varphi_N - \varphi_{N-1}}{t_N - t_{N-1}}\right]^T$$

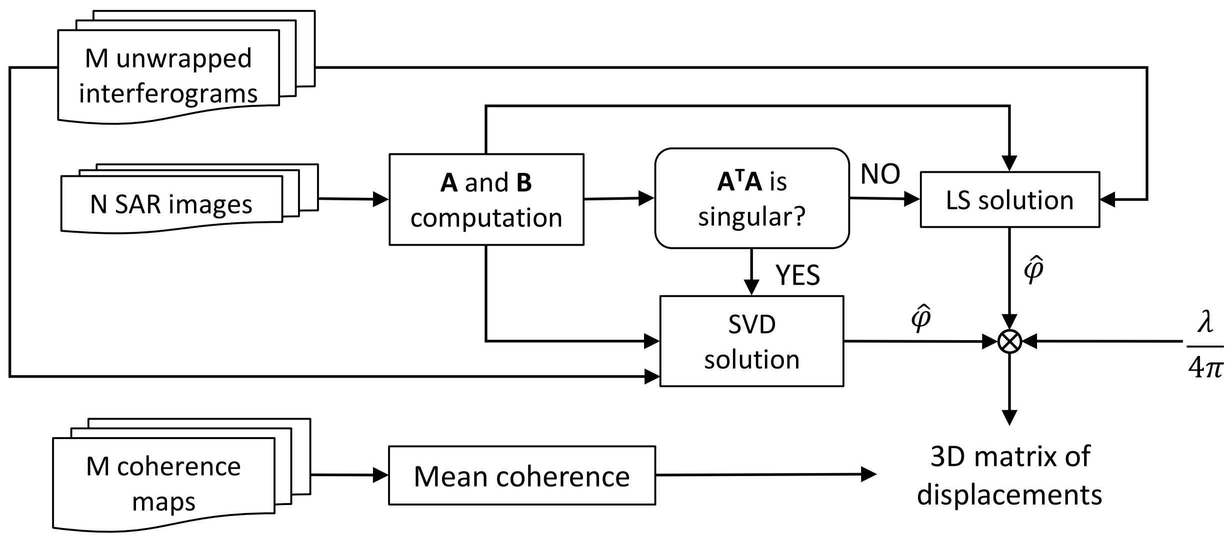

(1) Berardino, P., Fornaro, G., Lanari, R., & Sansosti, E. (2002). A new algorithm for surface deformation monitoring based on small baseline differential SAR interferograms. *IEEE Transactions on geoscience and remote sensing*, *40*(11), 2375-2383.

DInSAR Multi-Temporal Analysis
Methodology

- Deformation components:

$$\begin{cases} d_{asc} = \boldsymbol{d} \cdot \hat{\imath}_{asc} = d_H \sin\vartheta_{asc} + d_V \cos\vartheta_{asc} \\ d_{desc} = \boldsymbol{d} \cdot \hat{\imath}_{desc} = -\, d_H \sin\vartheta_{desc} + d_V \cos\vartheta_{desc} \end{cases}$$

- Matrix form:

$$\begin{bmatrix} d_{asc} \\ d_{desc} \end{bmatrix} = \begin{bmatrix} \sin\vartheta_{asc} & \cos\vartheta_{asc} \\ -\sin\vartheta_{desc} & \cos\vartheta_{desc} \end{bmatrix} \begin{bmatrix} d_H \\ d_V \end{bmatrix}$$

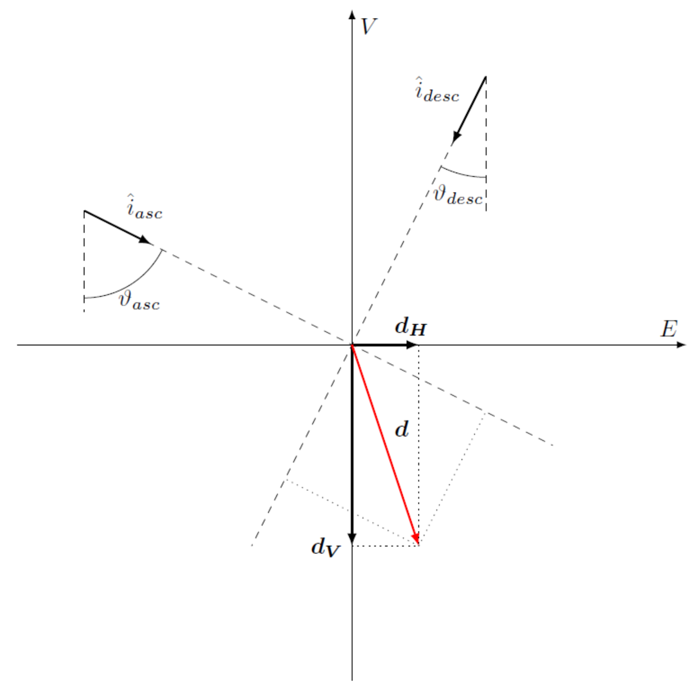

DInSAR Multi-Temporal Analysis

Implemented Algorithm

<u>Virtual Machine</u>:
- RAM: 32 GB
- HHD: 1 TB
- CPUs: 8

<u>Local Machine</u>:
- RAM: 16 GB
- SSD: 256 GB
- CPUs: 4

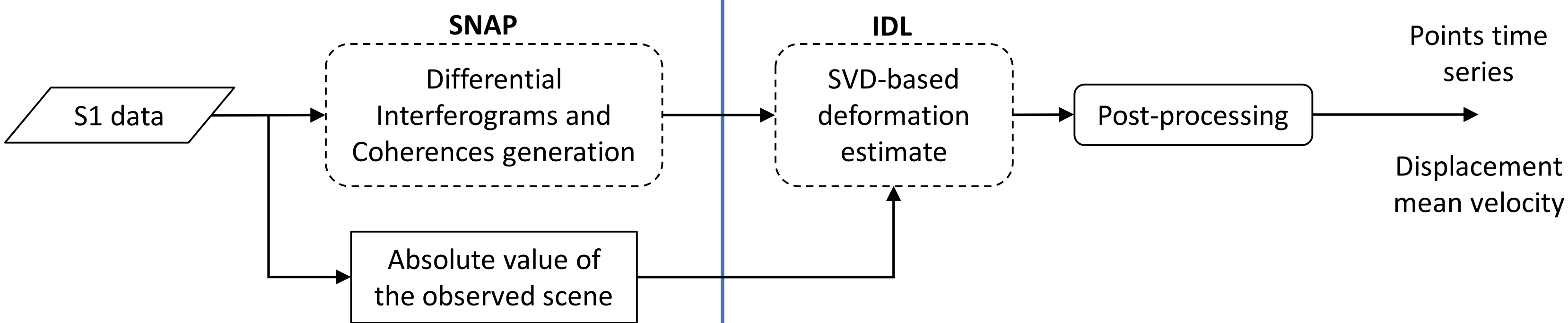

<u>SNAP</u>:
- Provides **multi-mission toolbox** for SAR and optical data.
- **Good integration** with other EO tool.
- **Free of charge** and **open source**.

<u>IDL</u>:
- EO **image processing**.
- **Good integration** with other applications.
- Access virtually **any type** of data.
- Requires license.

DInSAR Multi-Temporal Analysis

Results - Fiumicino Displacement maps

coherence values $\geq 0{,}4$

ascending track

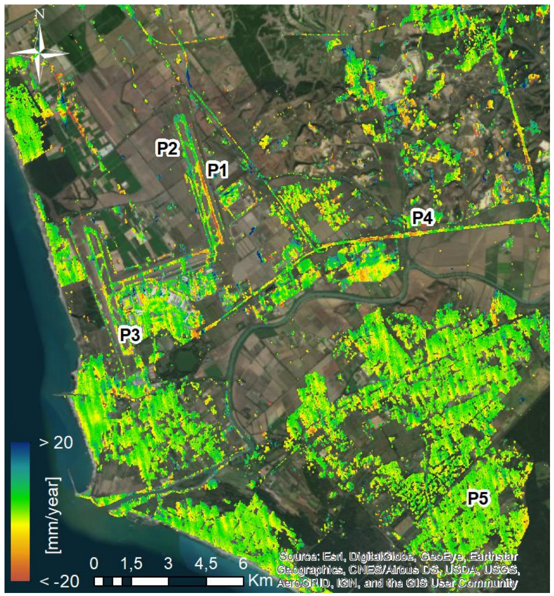

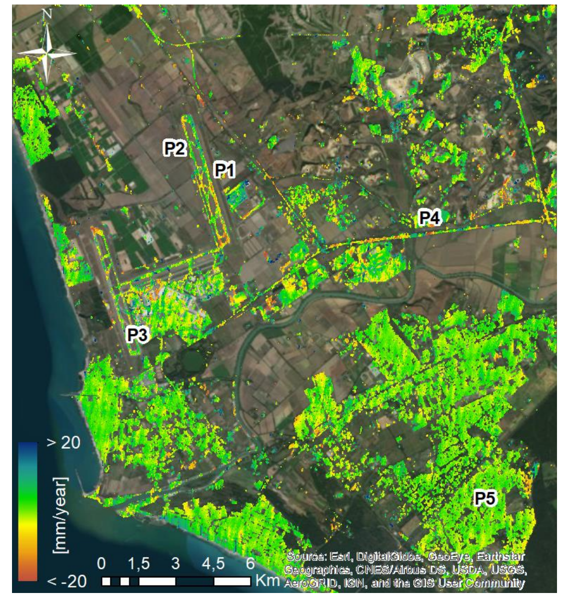

descending track

- **subsidence** ⟷ negative values ⟷ motion away from the sensor
- **uplift** ⟷ positive values ⟷ motion towards the sensor
- **reference area** ⟷ around P5 point ⟷ **man-made structures** (residential zones)

DInSAR Multi-Temporal Analysis

Results - Fiumicino Time Series

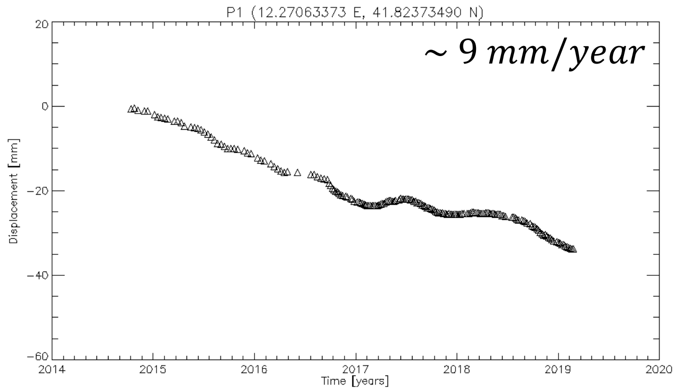

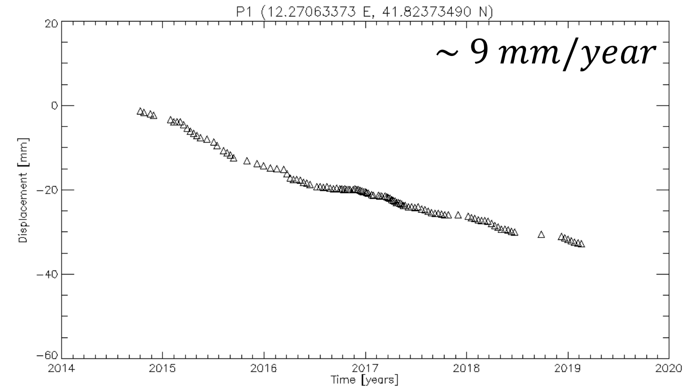

ascending track

descending track

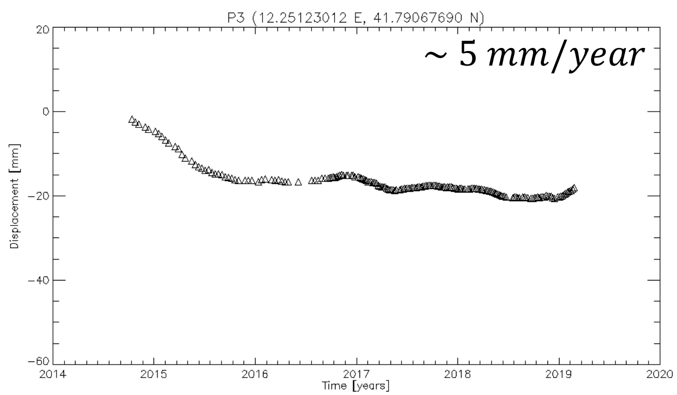

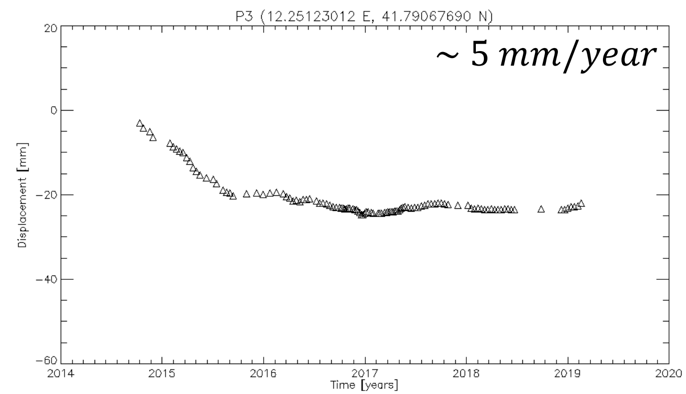

DInSAR Multi-Temporal Analysis

Results - Fiumicino Time Series

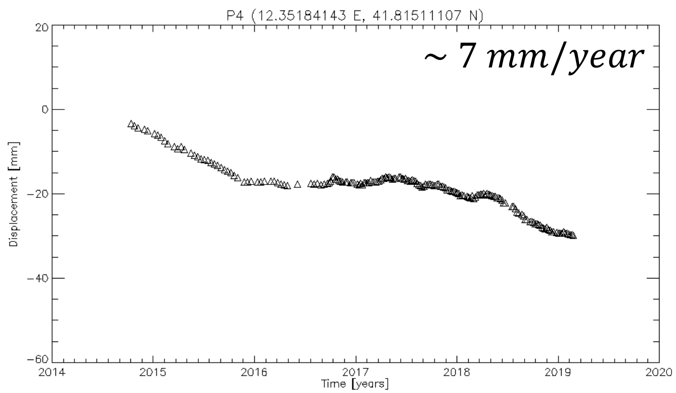

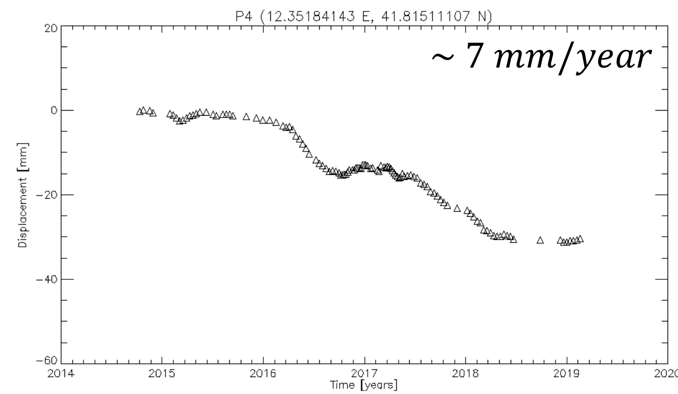

ascending track

descending track

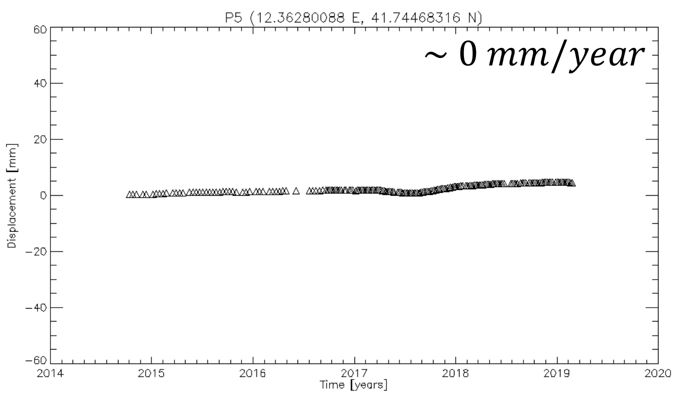

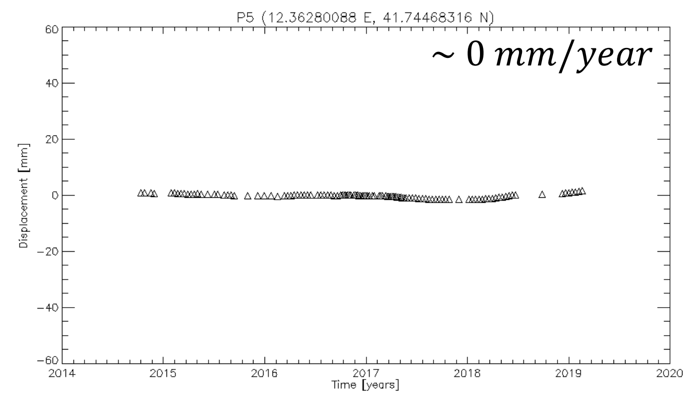

DInSAR Multi-Temporal Analysis

Results - Fiumicino (V, H) Displacement maps

coherence values $\geq 0{,}4$

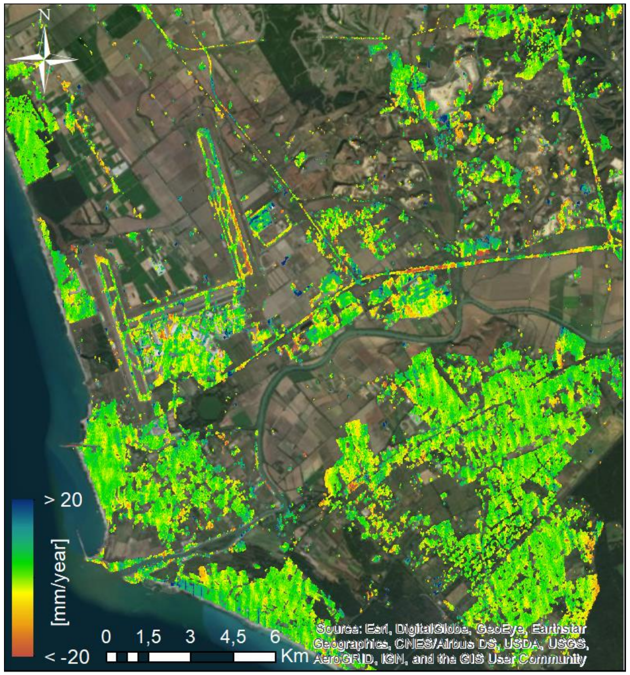

vertical component

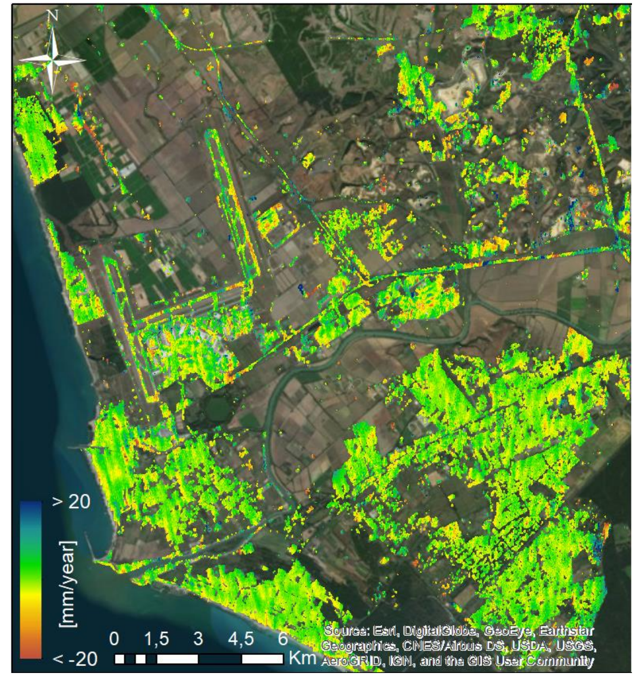

horizontal component

DInSAR Multi-Temporal Analysis

Results - Brumadinho Displacement maps

coherence values $\geq 0{,}4$

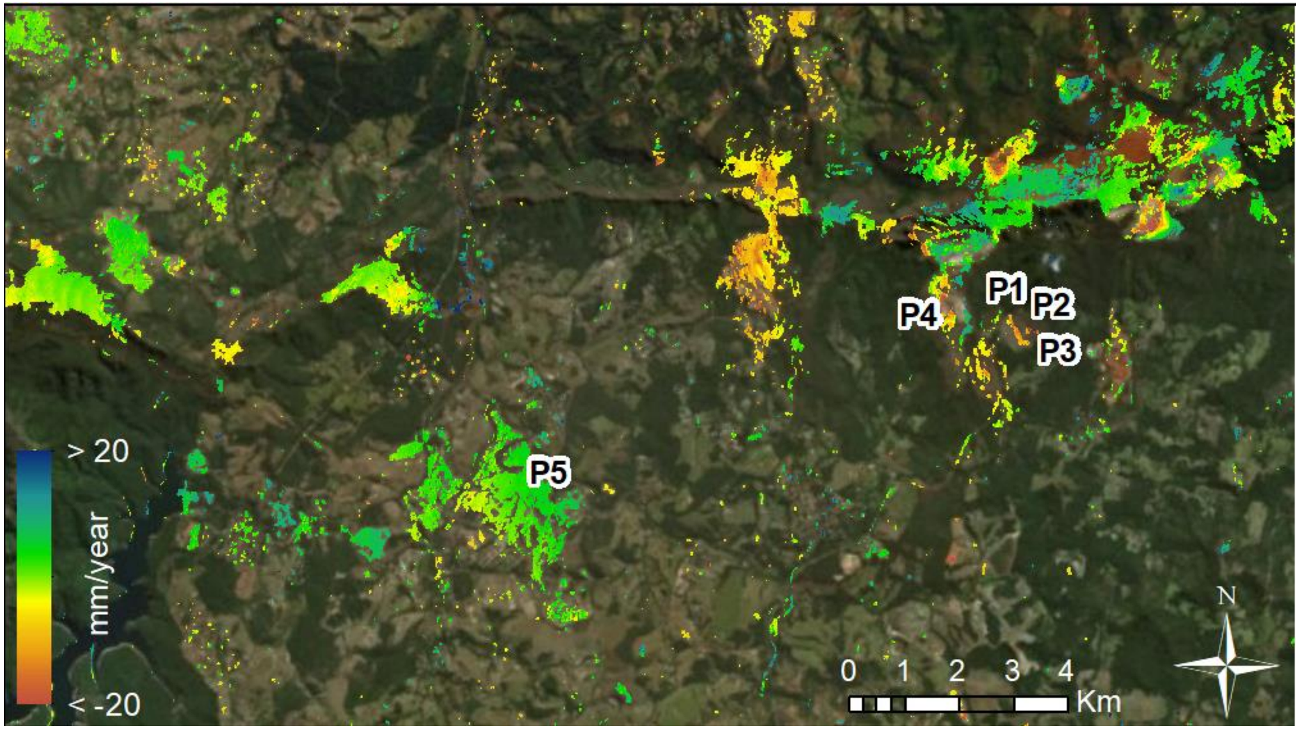

descending track

DInSAR Multi-Temporal Analysis

Results - Brumadinho Time Series

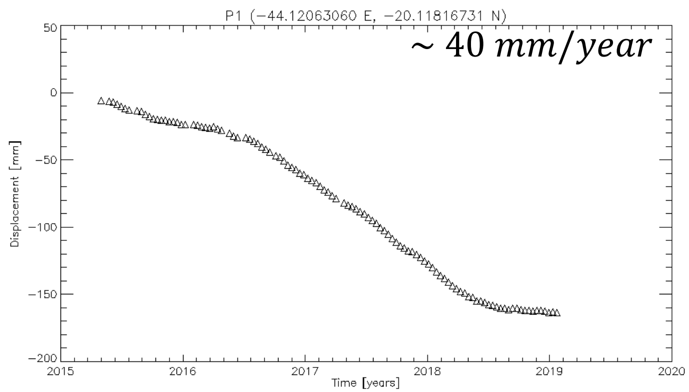

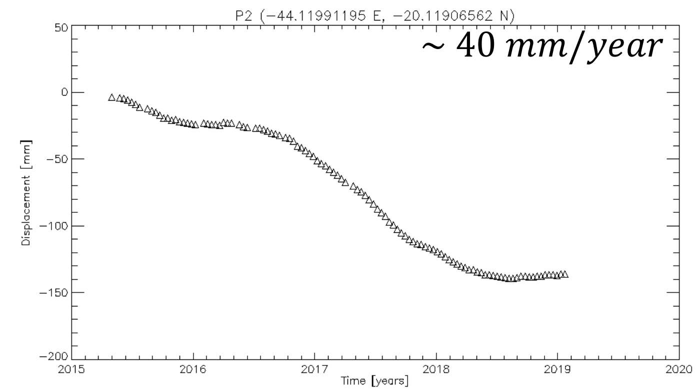

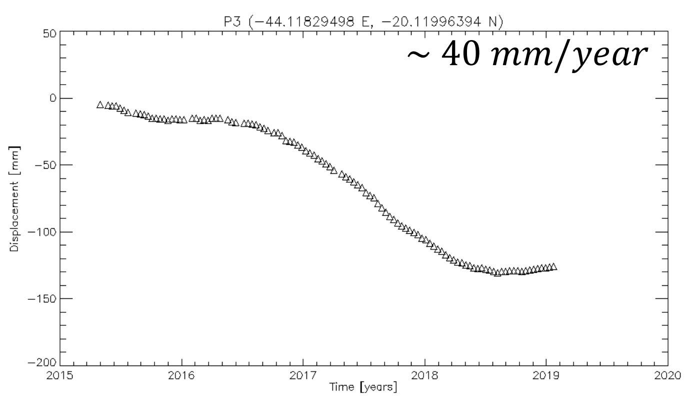

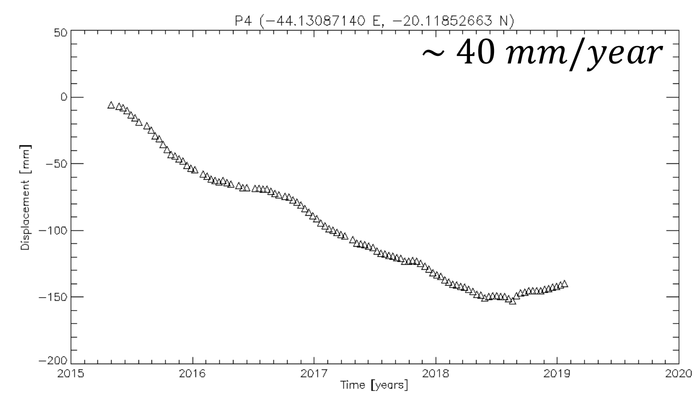

DInSAR Multi-Temporal Analysis

Activity Report

processed data storage

data [GB]	Fiumicino ascending	Fiumicino descending	Brumadinho descending	Total
Input	1480	912	864	3256
Intermediate	6368	1980	1418	9766
Output	2,7	1,5	1,5	5,7
Total	7850,7	2893,5	2283,5	13027,7

processing time

[min]	Fiumicino ascending	Fiumicino descending	Brumadinho descending
SNAP Tool	10,1	10,1	12,1
IDL Tool	7,0	5,0	5,0
Post-processing	0,8	0,5	0,5

- **Input data:** S1 IW SLC
- **Intermediate data:**
  - coregistered pairs
  - interferogram pairs
  - coherence maps
  - ⋮
- **Output data:**
  - 3D displacements matrix
  - time series
  - displacement maps
  - ⋮
- **SNAP Tool** ⟶ coregistered pair
- **IDL Tool** ⟶ all interferograms

Outline

Sub-Pixel Offset Tracking
Study Area

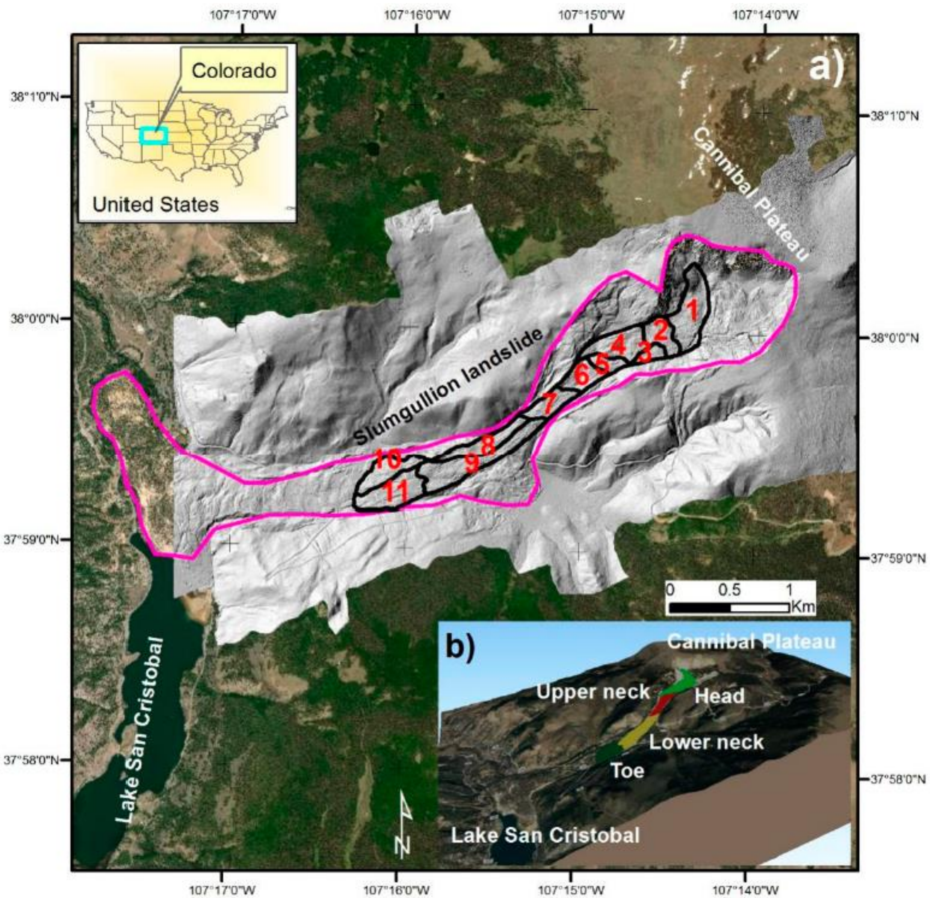

Slumgullion landslide, located in the San Juan Mountains, in southwestern Colorado, US.

It has been moving for about 350 years, with a maximum measured velocity of $6\ m$ per year.

It extends for about $7\ km$, from the Cannibal Plateau to Lake San Cristobal, with a mean width and depth of $300\ m$ and $14\ m$, respectively.

The area outlined in black ($1\ km$) is still active and it is constituted of 11 multiple kinematic elements, each of them moving like a rigid block sliding along faults.

Sub-Pixel Offset Tracking
Employed SAR data

Three COSMO-SkyMed spotlight images, about 1 m spatial resolution.
August 2011 - August 2012 - August 2013.

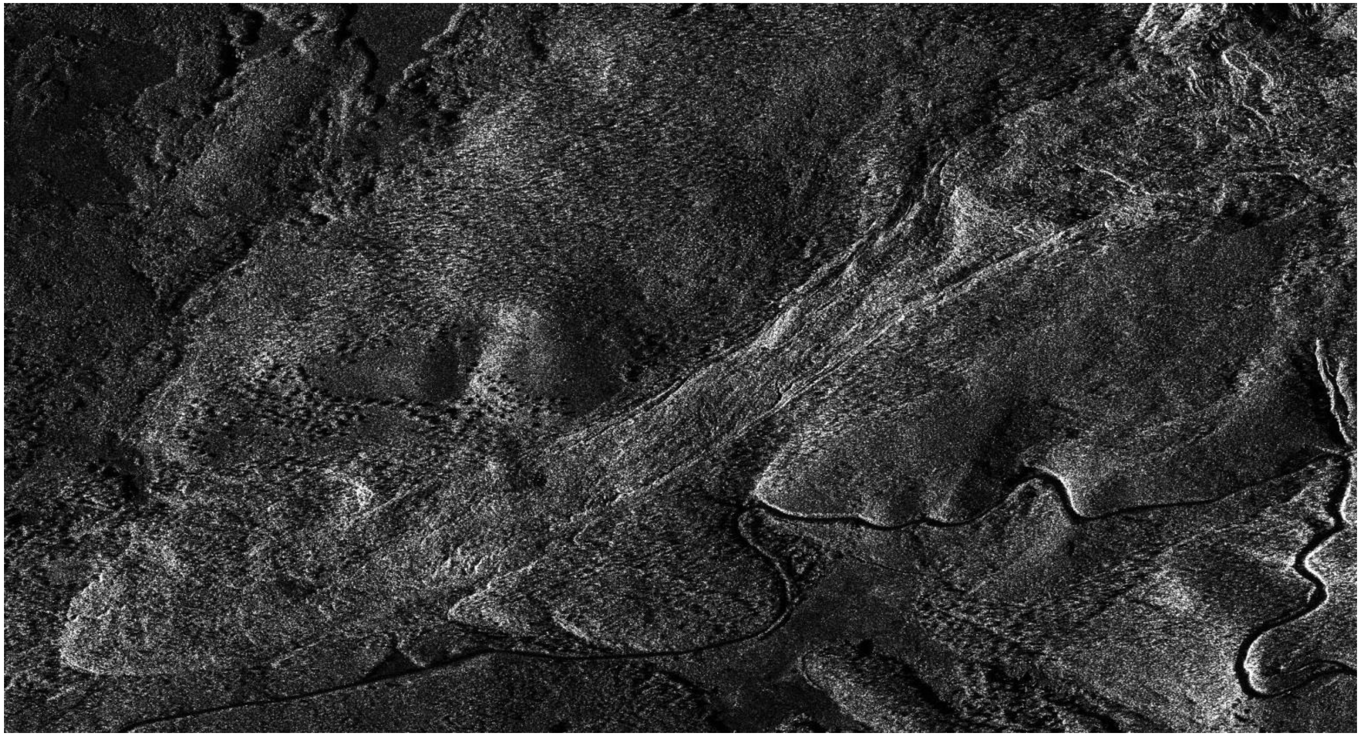

Sub-Pixel Offset Tracking

Methodology

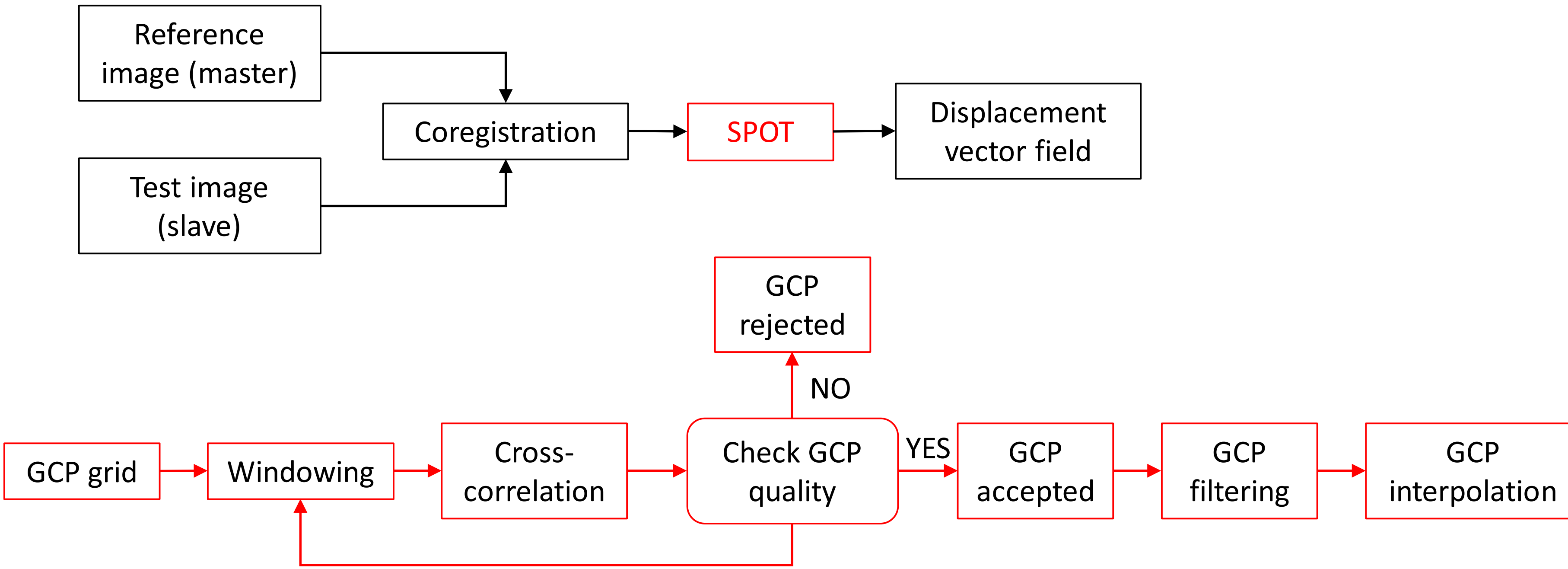

$$\boldsymbol{C} = \frac{\mathbb{F}^{-1}[\mathbb{F}[\boldsymbol{M}] \times \mathbb{F}[\boldsymbol{S}]^*]}{\sqrt{\langle \boldsymbol{M}^2 \rangle \times \langle \boldsymbol{S}^2 \rangle}} \qquad C_{ij} \in [0,1] \longrightarrow \text{Quality parameters: } \begin{cases} c_{max} \\ q = c_{max}/\langle \boldsymbol{C} \rangle \end{cases}$$

Sub-Pixel Offset Tracking

Results - Landslide Scale

August 2011-2012

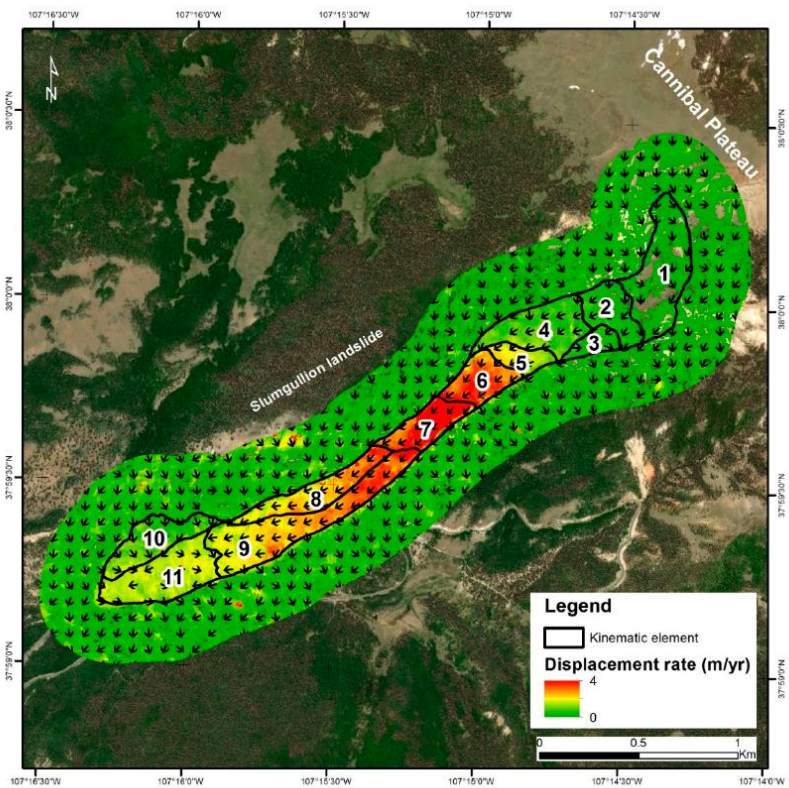

Setting parameters:

$f = 4$ → $\langle V \rangle_{min} = \begin{cases} 17\ cm & \text{azimuth} \\ 10\ cm & \text{range} \end{cases}$

$q_{thresh} = 4$

$C_{thresh} = 0{,}1$

$w = 64\ pixels$

The arrows represent the direction of the estimated vector field retrieved from the North–South and East–West components.

According to the past literature, the highest velocity values have been recorded in the central part of the landslide.

Sub-Pixel Offset Tracking

Results - Landslide Scale

c_{max} map August 2011-2012

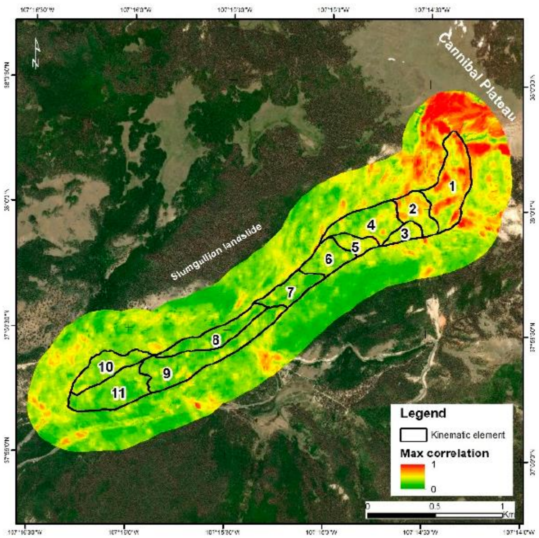

q map August 2011-2012

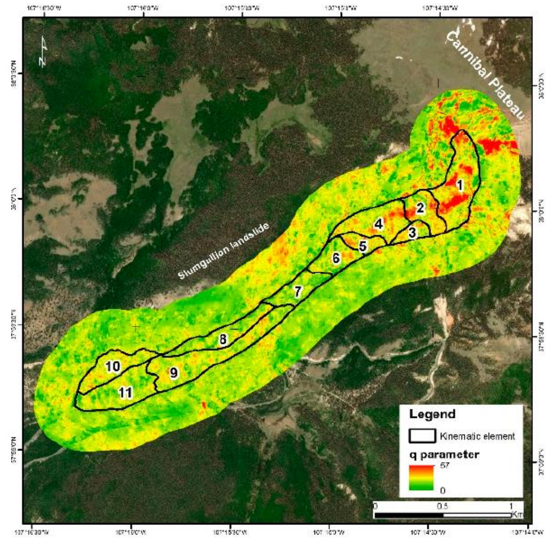

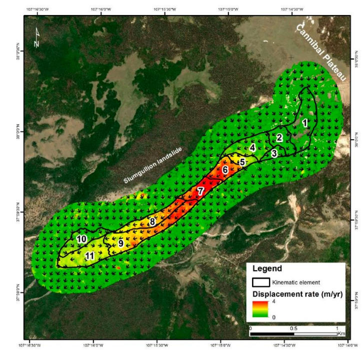

Setting parameters:

$f = 4$

$q_{thresh} = 4$

$C_{thresh} = 0{,}1$

$w = 64\ pixels$

The noisy displacement patterns correspond to areas with a low value of the considered quality parameters for the GCPs selection. This means that c_{max} is not well-defined compared with the background, thus leading to an unreliable estimate of the displacements. While, in the landslide area, q is quite high.

Sub-Pixel Offset Tracking

Numerical Results - Landslide Scale

Region ID	$\langle V \rangle$ 2011-2012	σ_V 2011-2012	$\langle V \rangle$ 2012-2013	σ_V 2012-2013	$\lvert CC \rvert$	σ_{CC}
			$w = 64$			
Landslide	1,03	0,79	0,81	0,72	0,01	0,42
1	0,11	0,09	0,13	0,08	0,07	0,14
2	0,26	0,13	0,16	0,09	0,00	0,15
3	0,33	0,13	0,24	0,10	0,03	0,19
4	0,54	0,18	0,38	0,16	0,08	0,19
5	1,11	0,29	0,91	0,29	0,12	0,23
6	2,00	0,49	1,80	0,42	0,09	0,63
7	2,40	0,67	2,14	0,55	0,07	0,89
8	1,56	0,47	1,24	0,45	0,05	0,50
9	1,63	0,47	1,34	0,59	0,09	0,52
10	0,58	0,23	0,36	0,16	0,09	0,30
11	1,00	0,17	0,52	0,18	0,05	0,26

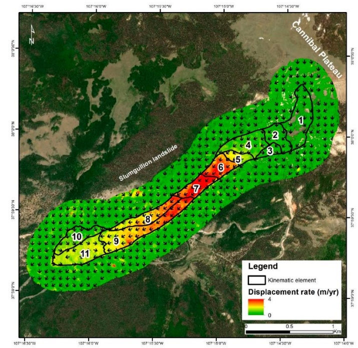

Setting parameters:

$f = 4$

$q_{thresh} = 4$

$C_{thresh} = 0{,}1$

$w = 64\ pixels$

A = 2011-2012 displacement map
B = 2012-2013 displacement map
C = 2011-2013 displacement map

↓

A + B – C = 0

Sub-Pixel Offset Tracking

Comparison with in-situ measurements

1985-1990 data from photogrammetry and field surveys
2010 data from Ground-Based SAR Interferometry

Region ID	$\langle V_f \rangle$ 1985-1990	σ_{V_f} 1985-1990	$\langle V_{GB} \rangle$ 2010	$\sigma_{V_{GB}}$ 2010	$\langle V \rangle$ 2011-2012	σ_V 2011-2012	$\langle V \rangle$ 2012-2013	σ_V 2012-2013
Landslide	2,48	1,38	1,16	1,35	1,03	0,79	0,81	0,72
1	0,73	0,40	0,14	0,91	0,11	0,09	0,13	0,08
2	1,20	0,25	0,32	1,27	0,26	0,13	0,16	0,09
3	1,42	0,14	0,36	1,31	0,33	0,13	0,24	0,10
4	1,60	0,51	0,36	0,98	0,54	0,18	0,38	0,16
5	2,44	0,29	1,05	1,53	1,11	0,29	0,91	0,29
6	3,86	0,87	1,67	2,51	2,00	0,49	1,80	0,42
7	5,25	0,73	2,84	3,35	2,40	0,67	2,14	0,55
8	3,57	0,40	1,64	3,13	1,56	0,47	1,24	0,45
9	3,65	0,87	1,93	3,06	1,63	0,47	1,34	0,59
10	1,56	0,18	0,91	6,49	0,58	0,23	0,36	0,16
11	1,97	0,36	1,13	2,37	1,00	0,17	0,52	0,18

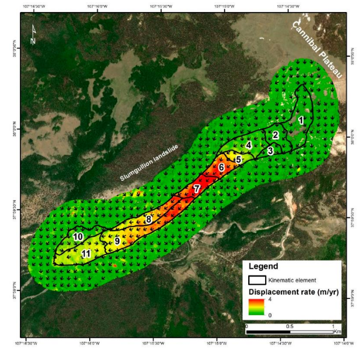

Setting parameters:

$f = 4$

$q_{thresh} = 4$

$C_{thresh} = 0{,}1$

$w = 64\ pixels$

The obtained displacement rates are consistent with that one of the GBInSAR survey implemented in 2010.

Sub-Pixel Offset Tracking
Results - Point Scale

- 19 MPs by the USGS: **GPS data**
- **Airborne L-band data** (time frame: August 2011-April 2012)
- **Our results**: $\langle V \rangle_{max}$ in a $100 \times 100\ m$ window around each MP

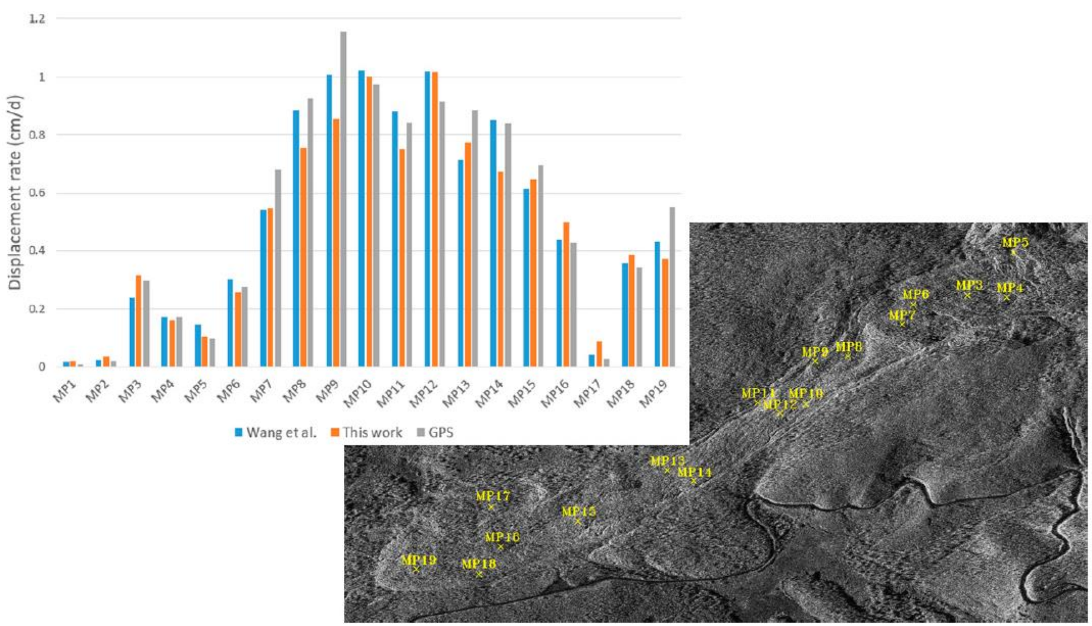

The three datasets qualitatively present a good agreement. Disagreements are grouped, as expected, in the neck area (MP8, MP9), where the landslide is faster. In fact, the landslide displacement rate is underestimated when compared to GPS data and to the measurements extracted from airborne SAR images

Outline

PART I

- Introduction
  - Remote Sensing and Synthetic Aperture Radar (SAR)
- SAR Acquisition Modes
  - Unified SAR Raw Signal Formulation
  - Application to Simulation: TOPSAR
  - Results and Computational Complexity

PART II

- Terrain Displacement Measurements via SAR
  - Introduction and Motivations
- DInSAR Multi-Temporal Analysis
  - Methodology and Implementation
  - Results
- Sub-Pixel Offset Tracking (SPOT) Technique
  - Methodology and Implementation
  - Results

CONCLUSIONS

Conclusions
Unified SAR Raw Signal Formulation

- Unified analytical formulation of the SAR raw signals of extended scenes, both in space and in frequency domains.
- Universal validity: applicable to all the SAR acquisition geometry.
- Simulation algorithm accounting for sensor trajectory deviations.
- More efficient than the available simulators, except for the cases in which a full 2D Fourier-domain approach is possible (i.e., stripmap, scanSAR and spotlight).
- Accuracy assessment:

  ✓ Time-Domain vs. Proposal for point targets

  ✓ Simulation of extended scenes, both canonical and real

  ✓ Computational complexity evaluation

Conclusions

Slow Landslides Monitoring by DInSAR

- DInSAR procedure for a preliminary study of the potential subsidence phenomena affecting two target sites.
- The presented results have confirmed that our approach provides displacement measurements in good agreement with those available in literature.
- The choice to generate a number of interferograms greater than the number of acquisitions (by means moving through a SBAS approach) has allowed us to
  - ✓ filter out the errors typically involved in the interferometric procedure
  - ✓ compensate for the possible temporal decorrelation effect
  - ✓ partially mitigate the atmospheric artifacts
- Drowback: partially automation of the processing chain

Conclusions
Fast Landslides Monitoring by SPOT

- SPOT is a feasible SAR technique, complementary to DInSAR.
- DInSAR: slow landslides (from cm/year to several cm/year).
- SPOT: fast landslides (> m/year) .
- Application of SPOT to monitor the Slumgullion landslide has been demonstrated.
- Consistency check and comparison with in-situ measurements support our results both at landslide and at point scale.
- Possible developments:
  - Space vs. frequency domain correlation computation
  - Automatic critera to set window size and quality parameters thresholds

List of Publications

International Conference Papers

[IC.1] **Dell'Aglio, D.**, Di Martino, G., Iodice, A., Riccio, D., & Ruello, G. (2018, July). Efficient Simulation of Extended-Scene SAR Raw Signals with Any Acquisition Mode. In *IGARSS 2018-2018 IEEE International Geoscience and Remote Sensing Symposium* (pp. 6715-6718). IEEE.

[IC.2] Amitrano, D., Costantini, M., **Dell'Aglio, D.**, Iodice, A., Malvarosa, F., Minati, F., ... & Ruello, G. (2018, September). Landslide Monitoring Using Sar Sub-Pixel Offset Tracking. In *2018 IEEE 4th International Forum on Research and Technology for Society and Industry (RTSI)* (pp. 1-4). IEEE.

[IC.3] Gargiulo, M., **Dell'Aglio, D. A. G.**, Iodice, A., Riccio, D., & Ruello, G. (2019, June). A CNN-Based Super-Resolution Technique for Active Fire Detection on Sentinel-2 Data. In *Progress In Electromagnetics Research Symposium (PIERS)* (pp. 1-8).

[IC.4] **Dell'Aglio, D. A. G.**, Gargiulo, M., Iodice, A., Riccio, D., & Ruello, G. (2019, September). Active Fire Detection in Multispectral Super-Resolved Sentinel-2 Images by Means of Sam-Based Approach. In *2019 IEEE 5th International forum on Research and Technology for Society and Industry (RTSI)* (pp. 124-127). IEEE.

[IC. 5] **Dell’Aglio D.A.G.**, Gargiulo M., Iodice A., Riccio D., Ruello G., “Fire Risk Analysis by using Sentinel-2 Data: The Case Study of the Vesuvius in Campania, Italy” submitted on IGARSS 2020.

List of Publications

National Conference Papers

[NC.1] **Dell’Aglio, D.**, Di Martino, G., Iodice, A., Riccio, D., Ruello, G. (2018, May). Efficient Simulation of SAR Raw Signals of Extended Scenes for Any Acquisition Mode. In *2nd Italian Radar and Remote Sensing Workshop (RRSW)* (pp. 1-4)

[NC.2] Amitrano, D., Costantini, M., **Dell'Aglio, D.**, Iodice, A., Malvarosa, F., Riccio, D., Ruello, G. (2018, July). Monitoring the Slumgullion landslide using SAR sub-pixel offset tracking. In *Conference of the Italian Society of Remote Sensing (AIT)* (pp. 1-4).

[NC.3] Gargiulo, M**., Dell’Aglio, D. A.**, Iodice, A., Riccio, D., & Ruello, G. (2019, October). Semantic Segmentation using Deep Learning: A case of study in Albufera Park, Valencia. In *2019 IEEE International Workshop on Metrology for Agriculture and Forestry (MetroAgriFor)* (pp. 134-138). IEEE

List of Publications

Journal Papers

[J.1] **Dell’Aglio, D. A.**, Di Martino, G., Iodice, A., Riccio, D., & Ruello, G. (2018). A Unified Formulation of SAR Raw Signals From Extended Scenes for All Acquisition Modes With Application to Simulation. *IEEE Transactions on Geoscience and Remote Sensing*, *56*(8), 4956-4967.

[J.2] Amitrano, D., Guida, R., **Dell’Aglio, D.**, Di Martino, G., Di Martire, D., Iodice, A., ... & Minati, F. (2019). Long-Term Satellite Monitoring of the Slumgullion Landslide Using Space-Borne Synthetic Aperture Radar Sub-Pixel Offset Tracking. *Remote Sensing*, *11*(3), 369.

Technical Note from Project Deliverables

[TN.1] **Dell’Aglio, D. A.**, (2019). Preliminary Multi-Temporal Analysis on Selected Targets. *Project: Monitoring Service Prototype through Automated Earth Observation Geo-Spatial Data Analyses using the Satellite Interferometry Technique*, Progressive Systems Srl, pp. 1-20.

Thank you for your kind attention